Polymer–metal–organic framework self-assembly (PMOFSA) as a robust one-step method to generate well-dispersed hybrid nanoparticles in water

Kun Li, Zhihao Yu, Iurii Dovgaliuk, Clémence Le Coeur, Viviane Lütz-Bueno, Eric Leroy, Blandine Brissault, Yoann de Rancourt de Mimerand, Mathilde Lepoitevin, Christian Serre, et al.

ChemComm

COMMUNICATION

Polymer–metal–organic framework self-assembly (PMOFSA) as a robust one-step method to generate well-dispersed hybrid nanoparticles in water†

Kun Li,[ab] Zhihao Yu,[c] Iurii Dovgaliuk,[c] Clémence Le Coeur,[abd] Viviane Lütz-Bueno,[de] Eric Leroy,[ab] Blandine Brissault,[ab] Yoann de Rancourt de Mimerand,[f] Mathilde Lepoitevin,[c] Christian Serre,[c] Jacques Penelle[ab] and Benoit Couturaud *[ab]

A new process, PMOFSA, is described here, that opens the way for the one-pot straightforward and versatile manufacture of polymer-MOF nanoparticles in water. It can be expected that this study will not only expand the scope of *in situ* preparation of polymer-MOF nano-objects but also inspire researchers in the field to prepare a new generation of polymer-MOF hybrid materials.

Metal–organic frameworks (MOFs) are ordered porous materials with adjustable morphologies as well as high surface areas. They have been prominently investigated in the last decade due to their excellent performance in gas storage,[1] separation,[2] sensing,[3] catalysis,[4,5] and biomedicine.[6,7] By varying the metals and organic ligands forming the scaffold, a large variety of MOFs can be synthesized, most of the time under conditions requiring organic solvents, and high temperatures and pressures.[8] Successful attempts at synthesizing them in water under conditions respectful of the environment rather than in organic solvents have been published recently.[9] One of the drawbacks of this method suggests that aggregation occurs during the process as the result of intrinsic MOF hydrophobicity. As a result, one-pot methodologies capable of fabricating MOF nanoparticles with good colloidal stability in water are under investigation.

Inspired by the PISA (polymerization-induced self-assembly) and CDSA (crystallization-driven self-assembly) processes used in polymer chemistry, a new methodology (PMOFSA or polymer–metal–organic framework self-assembly) is presented here that allows for the first time to reach the above objectives. Owing to many pioneering investigations, PISA[10–13] is today a commonplace nanofabrication process where the manufacture of amphiphilic polymers in water *via* an *in situ* hydrophobization of purely hydrophilic polymers progressively leads to the formation of polymeric nanoparticles of various morphologies, using the local phase separation of the introduced hydrophobic fragments as a driving force for the self-assembly. In the case of CDSA,[14–16] block copolymers composed of a solvophilic block and a semi-crystalline block are used. This technique exploits the ability of semi-crystalline polymers to self-assemble by the crystallisation of the core-forming block after heating above the melting transition temperature and cooling down in a poor solvent leading to stable anisotropic nanostructures.

By analogy, PMOFSAs (Scheme 1B) are envisioned as processes where the generation of increasingly hydrophobic MOF particles from water-soluble precursors underwent surface tethering by partially hydrophilic polymers, preventing aggregation and precipitation at an early growth step. In order to test

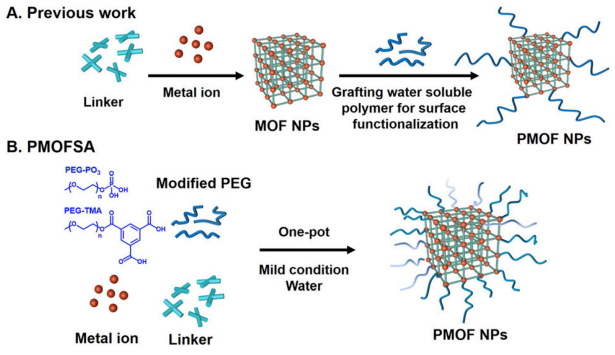

Scheme 1 Possible methods for the preparation of core–shell MOF nanoparticles stabilized by a hydrophilic polymer: (A) Two-step process, involving the successive synthesis of the MOF particles and their grafting.[22] (B) One-step approach according to the PMOFSA strategy presented here.

[a] *Univ Paris Est Créteil, ICMPE, UMR 7182, 2-8 rue H. Dunant, F-94320, Thiais, France. E-mail: benoit.couturaud@cnrs.fr*
[b] *CNRS, Institut de Chimie et des Matériaux Paris-Est (East Paris Institute of Chemistry & Materials Science), 2-8 rue H. Dunant, F-94320, Thiais, France*
[c] *Institut des Matériaux Poreux de Paris, ENS, ESPCI Paris, CNRS, Université PSL, 75005, Paris, France*
[d] *Laboratoire Léon Brillouin, CEA-CNRS (UMR-12), CEA Saclay, Université Paris-Saclay, 91191, Gif-sur-Yvette Cedex, France*
[e] *Paul Scherrer Institute, Forschungsstrasse 111, 5232, Villigen PSI, Switzerland*
[f] *Key Laboratory for Green Chemical Process of Ministry of Education, Wuhan Institute of Technology, Wuhan, 430205, China*
† Electronic supplementary information (ESI) available

the above concept, hydrophilic PEG (polyethylene glycol) polymers modified at one of their end-groups by a linking organic unit have been used in this study to stabilize iron(III)-based MOFs obtained from water-soluble trimesic acid (TMA) (1,3,5-benzenetricarboxylic acid) and iron(III) nitrate (Scheme 1). The resulting MOF is known as MIL-100(Fe). This solid is a benchmark MOF thanks to its high porosity, open metal sites (Lewis, redox), and biodegradable and biocompatible character, while its production can easily be scaled up under green conditions.[17] MIL-100(Fe) has been shown to exhibit great performances in a large array of potential applications from catalysis to separation of gases and biomedicine.[18–20] PEGs were selected because of their water solubility, non-toxicity and biocompatibility.[21]

Following the above approach, the resulting MOF core would be Fe(III) octahedral trimers and trimesate linkers, with PEG chains attached at the surface, as summarized in Scheme 1B. Such MOF structures are known but have only been obtained before by using two-step strategies that involve the synthesis of the MOF particles by classical methods in an organic solvent, followed by grafting of the PEG units on the surface of the obtained particles (A in Scheme 1).[20,23,24]

Prior to the self-assembly experiments, three modified PEGs of molecular weights 2k, 5k and 10k, containing a trimesic acid (TMA) end-group (PEG_{2k}-TMA, PEG_{5k}-TMA and PEG_{10k}-TMA) were synthesized by esterification of TMA with commercial PEGs that had only one hydroxyl end group PEG_{2k}-OH, PEG_{5k}-OH and PEG_{10k}-OH, respectively. A large excess of TMA was used to minimize multiple esterifications (see ESI†). An extra PEG, bearing another linker, a phosphate group (PEG-PO_3), was also synthesized. PEG-PO_3 was previously shown to bond strongly to MOF surfaces.[24] NMR spectroscopy and size exclusion chromatography data of the purified product (Fig. S1–S3, ESI†) suggest that the expected mono-ester is obtained as expected.

In practice, all starting materials are soluble in water and generate a continuous liquid phase at the beginning of the synthesis. MIL-100 (Fe) particles were synthesized by mixing Fe^{3+} ions with the TMA linker in water at 60 °C for 24 h with and without PEG. Table S1 (ESI†) summarizes the experimental variables: (a) the nature and molecular weight of the polymers (PEG_{2k}-TMA, PEG_{5k}-TMA, PEG_{5k}-PO_3, PEG_{10k}-TMA, PEG_{2k}-OH, PEG_{5k}-OH, PEG_{10k}-OH, and no polymer) and their amounts as expressed by their weight fractions in the initial water/PEG mixture. The resulting suspensions are indicated in the text by the PEG_x-OH/TMA/PO_3Y abbreviation, where x refers to the PEG molecular weight and Y to the PEG weight percent (wt%) in the initial water/PEG mixture.

The effect of the polymer on the outcome was univocal: all conditions that did not include PEG-TMA or PEG-PO_3 led to very unstable suspensions, with progressive precipitation of colored particles at the bottom of the vial and to very large aggregated particles in the supernatant as observed by TEM (Fig. 1A and Fig. S4, ESI†). As expected, based on the previous literature,[25] MIL-100 (Fe) nanoparticles tend to aggregate and yield large aggregates, with diameters of a few micrometers. For particles obtained with PEG_{2k}-OH, PEG_{5k}-OH particle aggregates are also large, with the solid precipitating out rapidly from the turbid solution (Fig. S4, ESI†).

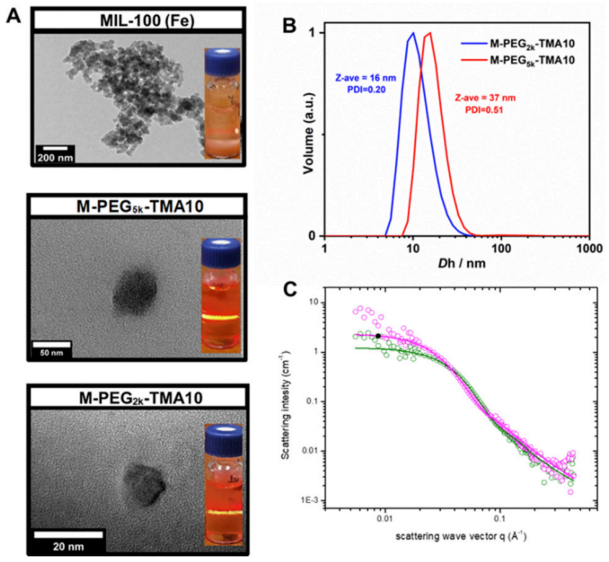

Fig. 1 (A) TEM of native MIL-100(Fe), M-PEG5k-TMA10 and M-PEG2k-TMA10, the insets correspond to images of the reaction mixtures after 24 h; (B) DLS and (C) SANS spectra of M-PEG2k-TMA10 and M-PEG5k-TMA10.

In contrast, Fig. 1 depicts typical results obtained in the presence of PEG-TMA, in comparison to bare MIL-100 (Fe). As shown by TEM in Fig. 1A, agglomerates were observed in the case of pristine MOF synthesis whereas disperse nanoparticles of M-PEG_{5k}-TMA10 and M-PEG_{2k}-TMA10 around 40 and 20 nm, respectively, were observed and exhibited good dispersity. The insets in the TEM image (Fig. 1A) show a homogenous colloidal solution for both PEG stabilized MOFs whereas pristine MOFs percolate to the bottom of the solution. Furthermore, NPs could be clearly observed in the supernatant liquid of M-PEG_{2k}-TMA10 and M-PEG_{5k}-TMA10 by a laser beam. DLS results confirmed the presence of small monodisperse particles with an average diameter of around 16 nm for M-PEG_{2k}-TMA10 and 37 nm for M-PEG_{5k}-TMA10 (Fig. 1B). Pure MOFs could not be measured by DLS as they are not colloidally stable in water. One day after the synthesis, the visual appearance of the dispersion, depicted in Fig. S5 (ESI†), shows dispersed hybrid particles without any sediment.

In comparison, we also used the classic two-step strategies that involve the synthesis of MOF particles followed by subsequent grafting of polymers on the surface of the MOF using PEG-TMA and PEG-PO_3 to obtain MOF-polymer particles in water. The DLS results can be seen in Table S1 (ESI†) denoted M@PEG. All the experiments led to bigger particles than the ones obtained from the PMOFSA method.

Several concentrations of M-PEG_{10k}-TMA, M-PEG_{5k}-TMA, M-PEG_{2k}-PO_3 and M-PEG_{2k}-TMA (1, 5, 10 and 15 wt%) were tested (Table S1, ESI†). A decrease in the hydrodynamic diameters while increasing PEG wt% is observed by DLS (Fig. S6, ESI†). TEM images for M-PEG_{5k}-TMA and M-PEG_{2k}-TMA (5, 10 and 15 wt%) corroborate the diameter decreases with the increase in PEG wt% (Fig. S7, ESI†). It clearly shows that the size tuning of the MOF particles can be achieved by increasing the wt%. The size of the PEG-TMA is also dependent on the PEG

molecular weight. This can be rationalised by the fact that a higher number of PEG chains stabilizes the MOFs.

SANS spectra of M-PEG$_{2k}$-TMA10 and M-PEG$_{5k}$-TMA10 are presented in Fig. 1C. SANS spectra were fitted by SASview software by a so called "polymer micelle model" corresponding to a dense core with a polymeric shell.[26] SANS spectra confirm that the obtained particles have a high stability and are hard core–polymeric shell spheres, as their curves fit perfectly to the model. Diameters measured by SANS are summarized in Table S2 (ESI†). There is a slight difference with the ones obtained from DLS measurements. This comes from the differences of size measurements between these two techniques. DLS measures the average hydrodynamic diameters, including the water layers associated with particle surfaces, while SANS assesses the static colloidal structure by measuring the internal core size distribution of particles and excluding the external water conjugation layer.[27]

The chemical composition and structure of the synthesized polymer-MOF nanoparticles were analyzed by Fourier transform infrared spectroscopy (FTIR), powder X-ray diffraction (PXRD), neutron scattering, high-resolution transmission electron microscopy (HR TEM) and X-ray photoelectron spectroscopy (XPS).

PXRD (Fig. S8, ESI†) confirmed the formation of a crystalline phase where the main reflection peaks (1.6–5.0° and 10.0–12.5°) matched those of native MIL-100, as expected.[18,28] Two new peaks centered at 2θ = 22.0° and 23.0° in ambient-dried M-PEG$_{2k}$-TMA10 and M-PEG$_{5k}$-TMA10 are due to the presence of amorphous and semicrystalline PEG. The first peak became broader in the presence of PEG-TMA. We reason that the ratio between PEG and crystalline core size is not in favor of defined PXRD data as previously described.[24,29] Nevertheless, TEM micrographs (Fig. 2) confirmed the formation of crystals, with two visible lattice distances of 0.25 and 0.21 nm.

Fig. S9 (ESI†) displays the XPS survey spectra for MIL-100 (Fe) and M-PEG$_{2k}$-TMA10, which indicate that both samples contain Fe, O, and C elements, as expected. The main peaks in Fig. S9 (ESI†) at 711.5 and 725.2 eV are characteristic of Fe 2p$_{3/2}$ and Fe 2p$_{1/2}$, with the peak at 718 eV attributed to Fe^{3+}.[30] These signals, in both MIL-100(Fe) and M-PEG$_{2k}$-TMA10, demonstrate that the iron species are predominantly Fe^{3+}. In the C 1s pattern of MIL-100(Fe) Fig. S9, ESI,† three peaks at 288.5, 285.8, and 284.5 eV can be deconvoluted and attributed to –COO, C═O and C–C bonds, respectively. The same three peaks appear in M-PEG$_{2k}$-TMA10 (Fig. S9, ESI†) but with the C═O/C–O–C combination signal much stronger than that of the –COO, in agreement with the increased content in the C–O–C and C–C bonds from PEG, significantly affecting the total balance. In the high-resolution O spectra of both MIL-100(Fe) (Fig. S9, ESI†) and M-PEG$_{2k}$-TMA10 (Fig. S9, ESI†), three peaks can be observed at 532.3 (532.4 in M-PEG$_{2k}$-TMA10), 531.6 (531.7), and 530.1 (529.9) eV, which are attributed to hydroxyls as well as adsorbed water, C–O/C═O bonds and Fe–O species in the crystal lattice, respectively. The ATR-FTIR spectra (Fig. S10, ESI†) of MIL-100(Fe), M-PEG$_{2k}$-OH10 and M-PEG$_{2k}$-TMA10 include a broad band centered around 3400 cm^{-1}, corresponding to O–H vibrations and a C═O stretching band at about 1730 cm^{-1}. The spectra of M-PEG$_{2k}$-TMA10 also include characteristic spectral features of poly(ethylene glycol) notoriously absent in the other samples: a CH_2 stretching vibration at 2885 cm^{-1} combined to a sharp, high intensity deformation band from the PEG C–O–C groups at 1098 cm^{-1}. In addition, the broad 3400 cm^{-1} signal (νO–H) almost disappears. In the M-PEG$_{2k}$-OH samples obtained after dialysis, the disappearance of the PEG chains could be ascertained by the fading of the –CH_2 vibration at 2885 cm^{-1} and a significant decrease in C–O–C vibration signals, a feature that was not observed for the M-PEG$_{2k}$-TMA10 sample. Finally, a few additional experiments were carried out to assess the scope and possible limitations of the above preparations. Attempts at changing the original temperature from 60 °C to 80 °C in M-PEG$_{2k}$-TMA10 led to a small increase in the particle diameter (from 19 to 27 nm), while experiments at 20 and 40 °C led to very large size distributions (Fig. S11, ESI†).

Finally, redispersion of M-PEG$_{2k}$-TMA10 dry powders obtained after freeze-drying was shown to be feasible, with the size parameters of the obtained suspension increasing slightly after 3 cycles compared to the initial system (Fig. S12, ESI†); this could be due to a limited collapse of the structure and aggregation through the freeze drying and redispersion process.

Finally, N_2 adsorption isotherms (77 K) of pristine MIL-100(Fe) obtained by vacuum drying (VAC) and freeze-drying (FD) have shown that freeze-drying can impair MIL-100(Fe) porosity (Fig. S13, ESI†). As M-PEG-TMA and M-PEG-PO3 can only be extracted by freeze-drying as they are too small and disperse, we could not access porosity of these systems. To assess whether the PMOFSA approach can be generalized to other MOF systems, the above procedure was used to produce stable Zr-MOFs in water with PEG$_{5k}$-TMA. Such solids are currently among the most studied MOF systems due to their versatility and good stability and have demonstrated their interest in catalytic and biomedical applications, among others.[31–33] Zr trimesate MOF-808 is a representative Zr-MOF due to its large 3D porosity and acidic metal sites. It can be noted that some of us recently succeeded in the production of well-defined monodispersed MOF-808 in aqueous solution-based solvents.[34] As expected based on the previous results described in this contribution, an enhanced colloidal stability was obtained using PEG$_{5k}$-TMA, which could be compared to solutions obtained in the absence of a TMA-modified PEG linker (Fig. S14, ESI†). Contrary to results obtained for MIL-100(Fe), the particle size did not change much in comparison with bare MOF-808, as shown in the TEM images in Fig. 3A and B. Based on DLS results, the hydrodynamic diameters for

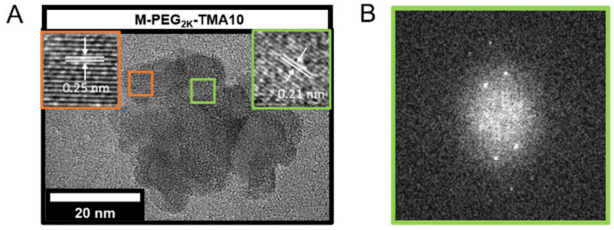

Fig. 2 (A) TEM micrographs of M-PEG$_{2k}$-TMA10, displaying two lattice distances (0.21 and 0.25 nm) and (B) FT image of the corresponding area of the M-PEG$_{2k}$-TMA10 TEM image.

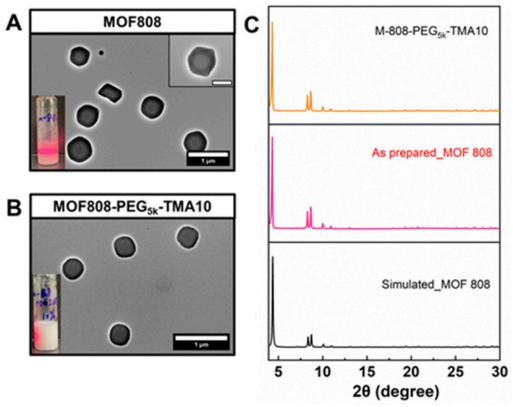

Fig. 3 (A) TEM micrograph of native MOF-808 (the inset shows a zoomed TEM image, scale bar = 200 nm); (B) TEM micrograph of MOF-808-PEG_{5k}-TMA10 (lower left insets for both A and B display the visual appearance of the dispersion state three days after the synthesis); (C) from bottom to top: PXRD diffractograms of simulated MOF-808, as-prepared MOF-808, and M-808-PEG_{5k}-TMA10.

M-808-PEG_{5k}-TMA10 and M-808-PEG_{5k}-TMA15 decreased slightly from 467.7 (±7.7) nm to 381.4 (±5.5) nm, respectively (Table S1, ESI†). PXRD demonstrated the successful synthesis of highly crystalline MOF-808 and MOF-808-PEG_{5k}-TMA10 by comparison to the simulated diffraction pattern (Fig. 3C). In summary, we present an efficient method to produce polymer-MOF hybrid materials synthesized by one-step polymer–metal–organic framework self-assembly (PMOFSA), which provides a facile and effective method to synthesize new polymer-MOFs. PEGs-TMA and PEG-PO_3 polymers promoted the MOF self-assembly. MOF-PEG-TMA hybrid polymer-MOFs displayed higher stabilization and well-dispersed nature than native MIL-100(Fe) and MOF-808(Zr). The PMOFSA process is a novel route that can promote a variety of potential applications in industry.

Finally, PMOFSA can be applied as a prospective strategy in different fields as it will bring the following benefits: a facile, ambient condition, and one-pot process to prepare well-dispersed NPs in water. Beyond a strong potential interest in biomedicine, the enhanced colloidal stability should be an asset for the use of these polymer-modified MOF NPs when preparing mixed matrix membranes for enhanced separation or new sensing devices. However, this work highlights that some challenges remain while performing one-step PMOFSA in aqueous solution. Future works will have to compromise between the colloidal stability, hybrid particle size and purification step to assess porosity measurements to obtain the best parameters that maintained porosity as the highest, while maintaining colloidal stability.

Conflicts of interest

There are no conflicts to declare.

Notes and references

1 Z. Chen, M. R. Mian, S.-J. Lee, H. Chen, X. Zhang, K. O. Kirlikovali, S. Shulda, P. Melix, A. S. Rosen, P. A. Parilla, T. Gennett, R. Q. Snurr, T. Islamoglu, T. Yildirim and O. K. Farha, *J. Am. Chem. Soc.*, 2021, **143**, 18838–18843.
2 H. Daglar, H. C. Gulbalkan, G. Avci, G. O. Aksu, O. F. Altundal, C. Altintas, I. Erucar and S. Keskin, *Angew. Chem., Int. Ed.*, 2021, **60**, 7828–7837.
3 H.-Y. Li, S.-N. Zhao, S.-Q. Zang and J. Li, *Chem. Soc. Rev.*, 2020, **49**, 6364–6401.
4 V. Pascanu, G. González Miera, A. K. Inge and B. Martín-Matute, *J. Am. Chem. Soc.*, 2019, **141**, 7223–7234.
5 L. Karam, M. C. Bacariza, J. M. Lopes, C. Henriques, J. Reboul, N. E. Hassan and P. Massiani, *J. CO2 Util.*, 2021, **51**, 101651.
6 X. Ma, M. Lepoitevin and C. Serre, *Mater. Chem. Front.*, 2021, **5**, 5573–5594.
7 T. Wen, G. Quan, B. Niu, Y. Zhou, Y. Zhao, C. Lu, X. Pan and C. Wu, *Small*, 2021, **17**, 2005064.
8 N. Stock and S. Biswas, *Chem. Rev.*, 2012, **112**, 933–969.
9 S. Dai, F. Nouar, S. Zhang, A. Tissot and C. Serre, *Angew. Chem., Int. Ed.*, 2021, **60**, 4282–4288.
10 F. D'Agosto, J. Rieger and M. Lansalot, *Angew. Chem., Int. Ed.*, 2020, **59**, 8368–8392.
11 N. J. W. Penfold, J. Yeow, C. Boyer and S. P. Armes, *ACS Macro Lett.*, 2019, **8**, 1029–1054.
12 H. Phan, V. Taresco, J. Penelle and B. Couturaud, *Biomater. Sci.*, 2021, **9**, 38–50.
13 J. C. Foster, S. Varlas, B. Couturaud, J. R. Jones, R. Keogh, R. T. Mathers and R. K. O'Reilly, *Angew. Chem., Int. Ed.*, 2018, **57**, 15733–15737.
14 L. MacFarlane, C. Zhao, J. Cai, H. Qiu and I. Manners, *Chem. Sci.*, 2021, **12**, 4661–4682.
15 J. R. Finnegan, E. H. Pilkington, K. Alt, M. A. Rahim, S. J. Kent, T. P. Davis and K. Kempe, *Chem. Sci.*, 2021, **12**, 7350–7360.
16 M. Inam, J. R. Jones, M. M. Pérez-Madrigal, M. C. Arno, A. P. Dove and R. K. O'Reilly, *ACS Cent. Sci.*, 2018, **4**, 63–70.
17 M. Panchal, F. Nouar, C. Serre, M. Benzaqui, S. Sene, N. Steunou and M. Giménez Marqués, *US Pat.* 17/242579, 2021.
18 P. Horcajada, S. Surblé, C. Serre, D.-Y. Hong, Y.-K. Seo, J.-S. Chang, J.-M. Grenèche, I. Margiolaki and G. Férey, *Chem. Commun.*, 2007, 2820–2822.
19 J. W. Yoon, Y.-K. Seo, Y. K. Hwang, J.-S. Chang, H. Leclerc, S. Wuttke, P. Bazin, A. Vimont, M. Daturi, E. Bloch, P. L. Llewellyn, C. Serre, P. Horcajada, J.-M. Grenèche, A. E. Rodrigues and G. Férey, *Angew. Chem., Int. Ed.*, 2010, **49**, 5949–5952.
20 M. Giménez-Marqués, E. Bellido, T. Berthelot, T. Simón-Yarza, T. Hidalgo, R. Simón-Vázquez, Á. González-Fernández, J. Avila, M. C. Asensio, R. Gref, P. Couvreur, C. Serre and P. Horcajada, *Small*, 2018, **14**, 1801900.
21 A. A. D'souza and R. Shegokar, *Expert Opin. Drug Delivery*, 2016, **13**, 1257–1275.
22 M. Kalaj, K. C. Bentz, S. Ayala, J. M. Palomba, K. S. Barcus, Y. Katayama and S. M. Cohen, *Chem. Rev.*, 2020, **120**, 8267–8302.
23 Z. Shi, X. Chen, L. Zhang, S. Ding, X. Wang, Q. Lei and W. Fang, *Biomater. Sci.*, 2018, **6**, 2582–2590.
24 X. Chen, Y. Zhuang, N. Rampal, R. Hewitt, G. Divitini, C. A. O'Keefe, X. Liu, D. J. Whitaker, J. W. Wills, R. Jugdaohsingh, J. J. Powell, H. Yu, C. P. Grey, O. A. Scherman and D. Fairen-Jimenez, *J. Am. Chem. Soc.*, 2021, **143**, 13557–13572.
25 A. Zimpel, T. Preiß, R. Röder, H. Engelke, M. Ingrisch, M. Peller, J. O. Rädler, E. Wagner, T. Bein, U. Lächelt and S. Wuttke, *Chem. Mater.*, 2016, **28**, 3318–3326.
26 J. Pedersen, *J. Appl. Crystallogr.*, 2000, **33**, 637–640.
27 F. Bouanani, D. Bendedouch, C. Maitre, J. Teixeira and P. Hemery, *Polym. Bull.*, 2005, **55**, 429–436.
28 B. E. Souza, A. F. Möslein, K. Titov, J. D. Taylor, S. Rudić and J.-C. Tan, *ACS Sustainable Chem. Eng.*, 2020, **8**, 8247–8255.
29 Y. Gu, M. Huang, W. Zhang, M. A. Pearson and J. A. Johnson, *Angew. Chem., Int. Ed.*, 2019, **58**, 16676–16681.
30 X. Zheng, L. Zhang, Z. Fan, Y. Cao, L. Shen, C. Au and L. Jiang, *Chem. Eng. J.*, 2019, **374**, 793–801.
31 F. Demir Duman, A. Monaco, R. Foulkes, C. R. Becer and R. S. Forgan, *ACS Appl. Nano Mater.*, 2022, 13862–13873.
32 B. Bohigues, S. Rojas-Buzo, M. Moliner and A. Corma, *ACS Sustainable Chem. Eng.*, 2021, **9**, 15793–15806.
33 A. M. Rabon, J. G. Doremus and M. C. Young, *Tetrahedron*, 2021, **85**, 132036.
34 S. Dai, C. Simms, I. Dovgaliuk, G. Patriarche, A. Tissot, T. N. Parac-Vogt and C. Serre, *Chem. Mater.*, 2021, **33**, 7057–7066.